2D and 3D TCAD Simulation of III-V Channel FETs at the End of Scaling

P. Aguirre, M. Rau, and A. Schenk

Integrated Systems Laboratory, ETH Zurich, Gloriastrasse 35, 8092 Zurich, Switzerland

Abstract

Quantum drift diffusion corrections, models for the one- and two-dimensional density of states, a non-local model for source-to-drain tunneling, and a simple ballistic mobility model are jointly used to simulate $I_D V_{GS}$-characteristics of scaled III-V-channel nFETs. The sub-threshold swing of double-gate ultra-thin-body and gate-all-around nanowire geometries are extracted for different gate lengths, and the semi-classical results are compared with those from the quantum transport simulator QTx. The low-dimensional density of states in combination with the ballistic mobility yields an overall good agreement with the QTx transfer curves after the onset of inversion and decreases I_{ON} by two orders of magnitude in comparison to the simulation with a large diffusive mobility. It is shown that source-to-drain tunneling sets a limit to scaling at a gate length of about 10 nm due to the degradation of the sub-threshold swing. Simulating this effect with a low-dimensional density of states reveals inconsistencies. They are attributed to the tunneling model, which had been derived for a three-dimensional electron gas.

1. Introduction

The high electron mobility and injection velocity of III-V-compounds-based FETs make them promising candidates to replace n-type strained Si MOSFETs at future technology nodes with gate lengths shorter than 20 nm [1]. The aggressive scaling causes quantum effects which have a critical influence on the device performance. For instance, geometrical quantum confinement in the body with thickness (t_{body}) below 12 nm leads to a shift in the threshold voltage [2]. Moreover, at gate lengths shorter than 20 nm, the potential barrier between source and drain becomes thin enough, so that source-to-drain tunneling (STDT) deteriorates or even determines the sub-threshold swing (*SS*) [3]. Quantum transport (QT) simulators start to find their way into industrial environments, however, they are computational expensive for large and complex 2D and 3D devices [4]. In this paper, it is systematically shown how quantum drift diffusion (QDD) tools [5] in combination with a TCAD-friendly ballistic mobility model [6, 7] can be used to simulate the described quantum effects. A reasonable agreement with QT simulation results is achieved for *SS*, but I_{ON} is still too high in the linear regime.

Table 1: Dimensions of the GAA NW FETs according to future technology nodes as described in [12].

Node	L_G [nm]	t_{ox} [nm]	t_{body} [nm]	m_e/m_0	α_{np}
A	15	3.75	7	0.0642	1.2
B	10.4	3.25	5.5	0.0674	1.1

2. Simulation Approaches

First, 2D simulations of the double-gate ultra-thin-body (DG UTB) transistor shown in Fig. 1 (a) were performed using the quantum transport code QTx [8]. The same geometry with t_{body} = 7 nm was simulated for different L_G ranging from 10 nm to 25 nm. Next, 3D simulations using QTx were done for gate-all-around nanowire (GAA NW) FETs. Their design parameters are the same as for the DG UTB FETs. The dimensions are given in Tabel 1. The $I_D V_{GS}$-characteristics simulated with QTx were used as reference to calibrate the QDD simulation setup of the commercial simulator Sentaurus-Device (S-Device) [9]. Effective masses were calculated from a full-band version of the QT code [10]. QTx itself is an effective-mass version, which takes advantage of a calibrated non-parabolicity parameter to best reproduce the real band structure [8].

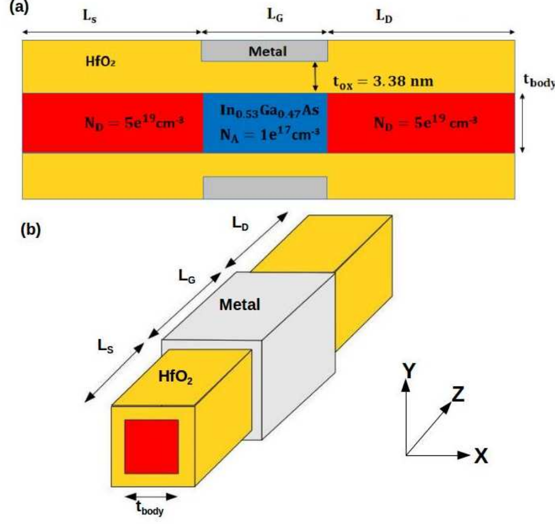

Figure 1: Schematic of (a) $In_{0.53}Ga_{0.47}As$ double-gate ultra-thin-body (DG UTB) FET and (b) $In_{0.53}Ga_{0.47}As$ gate-all-around nanowire (GAA NW) FET.

2.1. Geometrical Confinement and Source-to-drain Tunneling

To simulate the effect of confinement perpendicular to the transport direction in the 2D and 3D structures two models can be used:

(i) The Density Gradient (DG) Model, which adds a quantum potential (Λ) in the computation of the carrier density (n). This model depends on ∇n, m_e and a fitting parameter γ. The latter can be found by a Schrödinger-Poisson solver [4] using the 1D electron density profile along a vertical cut in the middle of the device.

In the 3D simulations of the GAA NWs we applied the anisotropic DG model which uses an attenuation matrix with diagonal elements α_l, α_v in order to scale Λ in longitudinal and vertical direction, respectively. The element α_v serves to reproduce the confinement effect perpendicular to the transport direction, whereas the α_l-value smoothens the energy barrier between source and drain. The fitting parameter γ for both transverse directions (x and y) was calibrated using the 1D density profile in the center of the GAA NW along the y-direction in the middle yz-plane (compare Fig. 1). The QTx electron density profile along the same line was taken as reference. By matching the densities at zero drain bias over the entire V_{GS}-range, the electrostatics can be fitted *independently of the mobility model used*. Note that in TCAD simulations of MOSFETs the work function (WF) is always considered as adjustable parameter.

(ii) The Modified Local Density Approximation (MLDA), without any fitting parameter [15].

For the simulation of STDT there are two options:

(i) The Nonlocal Tunneling (NLT) model [5] in combination with the MLDA and the anisotropic DG model (applied to the transverse direction), respectively. In the latter case $\alpha_l = 0$ has to be chosen. The tunneling mass has to be set to a proper value extracted from the QT solver. The NLT model computes the semi-classical barrier tunneling current using distribution functions with local quasi-Fermi potentials (QFPs) at the classical turning points [9]. The formula has been derived for a 3D electron gas (3DEG).

(ii) The anisotropic DG model applied to the transport direction. FETs with ultra-short gates also have steep density gradients along the channel. The computed quantum correction smoothens the source-to-drain potential barrier and induces an additional drift-diffusion current which mimics the tunnel current.

2.2. Density of States and Fermi Correction to the Current Density

The default DOS model in S-Device is that for a 3DEG:

$$N_c^{3D} = \frac{1}{\sqrt{2}}\left(\frac{m_c k_B T}{\pi\hbar^2}\right)^{3/2} . \quad (1)$$

Here, m_c is the DOS effective mass and k_B the Boltzmann constant. For the simulation of low-dimensional devices also 2DEG/1DEG DOS models are available [9, 17] which can be used in combination with Fermi statistics. In the devices under study, side valleys are negligible [18], only the Γ-valley is populated. The simulator provides a 'Multivalley' option, i.e. the 3DEG can be distributed over multiple valleys. Here, we use this framework for the sub-bands (subscript i) that are generated by size quantization of the 3DEG in the Γ-valley. The corresponding three-dimensional electron densities (in units cm^{-3}) are computed with the expressions

$$n_{2DEG} = \sum_i N_c^{3D}\left(m_i^{2D}\right) F_0\left(\eta, \epsilon_i, \alpha_{np,i}\right) , \quad (2)$$

$$n_{1DEG} = \sum_i N_c^{3D}\left(m_i^{1D}\right) F_{-\frac{1}{2}}\left(\eta, \epsilon_i, \alpha_{np,i}\right) . \quad (3)$$

Here, $F_p\left(\eta, \epsilon_i, \alpha_{np,i}\right)$ is the generalized Fermi integral

$$F_p\left(\eta, \epsilon_i, \alpha_{np,i}\right) = \int_0^\infty d\epsilon \frac{[\epsilon(1 + k_B T \alpha_{np,i}\epsilon)]^p (1 + 2k_B T \alpha_{np,i}\epsilon)}{1 + \exp(\epsilon + \epsilon_i - \eta)} \quad (4)$$

with $\eta = (E_{F,n} - E_c)/k_B T$ and $\epsilon_i = \Delta E_{n,i}/k_B T$. The latter is the normalized sub-band energy referenced to

the bulk band edge E_c. The mass parameters $m_i^{2D,1D}$ are derived from the actual quantization masses $m_{qu,i}^{2D,1D}$ by the transformations

$$m_i^{2D} = \left(\frac{m_{qu,i}^{2D}}{t_{body}}\right)^{2/3} \left(\frac{2\pi\hbar^2}{k_B T}\right)^{1/3}, \quad (5)$$

$$m_i^{1D} = \left(\frac{m_{qu,i}^{1D}}{t_{body}}\right)^{1/3} \frac{1}{t_{body}} \left(\frac{\pi\hbar^2}{k_B T}\right)^{2/3}. \quad (6)$$

110 They ensure that the prefactors in Eqs. (2) and (3) yield correct effective densities of states when N_c^{3D} from Eq. (1) is used. The parameter $\alpha_{np,i}$ accounts for the non-parabolicity of each sub-band.

The condition that the drift-diffusion current must vanish at equilibrium also when Fermi statistics is required leads to a Fermi correction term in the equation for the current density [9]:

$$j_{FS} = -\mu_n n k_B T \nabla \ln(\gamma_n) \qquad \gamma_n = n/n_B, \quad (7)$$

where n is one of the densities Eq. (2) or Eq. (3) and n_B
115 their Boltzmann limit. The correction term is negative, hence at high V_{GS} the current density is reduced when the quasi-Fermi level moves into the first sub-band. The term has, therefore, the same effect as a ballistic mobility correction. Before one can make any statements
120 about the latter, a careful calibration of the DOS is necessary.

There are two possibilities to fit the 2DEG/1DEG DOS in S-Device. The first one is to extract the sub-band energies $\Delta E_{n,i}$, the quantization masses $m_{qu,i}^{1D,2D}$,
125 and the non-parabolicity parameters $\alpha_{np,i}$ of the populated sub-bands from the QTx dispersion curves. From the quantization masses needed for the input file the mass parameters $m_i^{1D,2D}$ are computed internally. The second possibility is to fit the DOS by matching the
130 QV_{GS}-curves of QTx and S-Device in the inversion regime. Naturally, one can only fit *one* parameter. The best way is to take the sub-band energies $\Delta E_{n,i}$ and the non-parabolicity parameter α_{np} from QTx (only a single α_{np} is needed to fit the QTx effective-mass band struc-
135 ture to the real band structure) and to calibrate a mass parameter $\langle m_{qu}^{1D,2D}\rangle$ which is then used for all sub-bands. It represents a certain average over all $m_{qu,i}^{1D,2D}$ obtainable from QTx.

2.2.1. 2DEG DOS

140 To determine the work function and the input parameter $\langle m_{qu}^{2D}\rangle$ for the 2DEG DOS, the DG UTB FET of Fig. 1(a) was simulated at $V_{DS} = 0$ V both with QTx and S-Device, including 4 sub-bands.

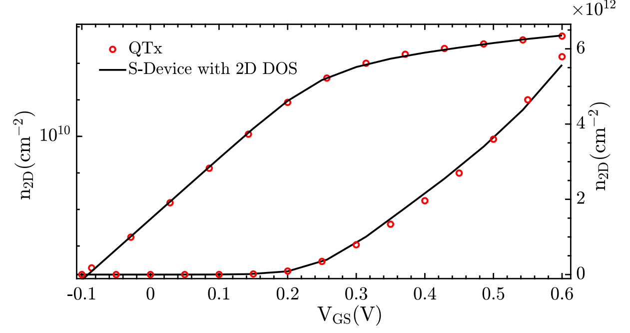

Figure 2: 2D electron density at the center of the channel vs. gate voltage in the DG UTB FET with t_{body} = 7 nm and L_G = 40 nm at V_{DS} = 0 mV. The threshold voltage was fitted including 4 sub-bands with $\langle m_{qu}^{2D}\rangle$ = 0.038 m$_0$ and α_{np} = 1.17 eV^{-1} which gives a value of 4.78 eV for the WF.

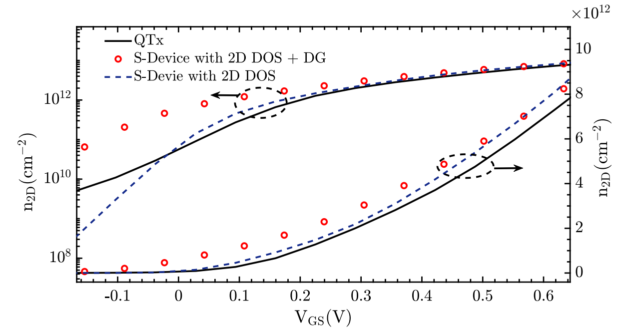

Figure 3: 2D electron density at the center of the channel vs. gate voltage in the DG UTB FET with t_{body} = 7 nm and L_G = 15 nm at V_{DS} = 0 mV. Parameters: $\langle m_{qu}^{2D}\rangle$ = 0.027 m$_0$, α_{np} = 1.17 eV^{-1}, WF = 4.78 eV, γ = 0.7, and (α_l, α_v) = (0.8, 0).

First, to minimize the effect of quantum-mechanical
145 charge penetration into the source-to-drain potential barrier and to make the fitting of the WF feasible, a long gate with L_G = 40 nm was chosen. The good match of the two QV_{GS}-curves in the sub-threshold and inversion regimes is shown in Fig. 2.

150 Next, we used the values of the WF and $\langle m_{qu}^{2D}\rangle$ obtained from the previous calibration and simulated QV_{GS}-curves for shorter gate lengths. Because STDT determines the SS at those gate length, the corresponding charge penetration into the barrier at equilibrium
155 (V_{DS} = 0) also changes the slope of the QV_{GS}-curves in the sub-threshold range. Fig. 3 presents the case of L_G = 15 nm. It shows that the slope of the QTx-curve cannot be reproduced without a quantum correction in S-Device. Since the NLT model is only active when
160 V_{DS} > 0, the only way is to apply the anisotropic DG model in transport direction and to fit the value of α_l.

2.2.2. 1DEG DOS

To determine the work function and the input parameter $\langle m_{\rm qu}^{\rm 1D}\rangle$ for the 1DEG DOS, the GAA NW FET of Fig. 1(a) was simulated at $V_{\rm DS} = 0\,{\rm V}$ both with QTx and S-Device including 5 sub-bands. In order to minimize the effect of quantum-mechanical charge penetration into the source-to-drain potential barrier and to make the fitting of the WF feasible, a gate length of $L_{\rm G} = 30\,{\rm nm}$ is sufficient here (stronger source-to-drain barrier due to GAA architecture). A good agreement between the two $QV_{\rm GS}$-curves is achieved as shown in Fig. 5. Fig. 4 shows the extracted QTx band diagram at

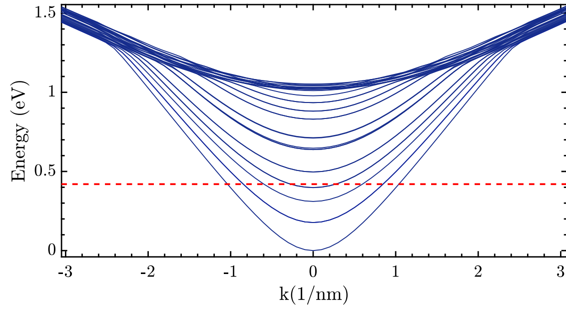

Figure 4: Band diagram calculated at a point in the heavily doped source of the 3D GAA NW FET with $t_{\rm body} = 7\,{\rm nm}$. The dashed red line shows the position of the Fermi level.

a point in the heavily doped source of the 3D GAA NW used for calibration. In the simulations with S-Device 6 sub-bands were included, with $\Delta E_{\rm n,i}$ set to the value of the minimum of the ith sub-band.

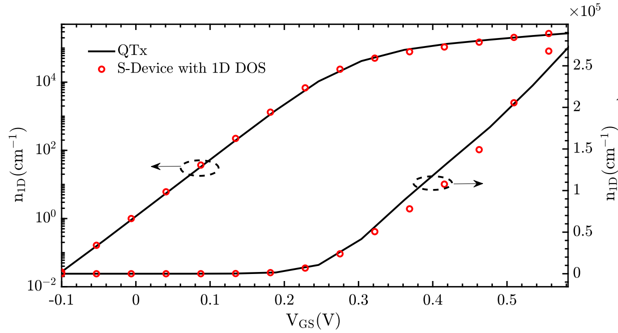

Figure 5: 1D electron density at the center of the channel vs. gate voltage in the GAA NW FET with $t_{\rm body} = 7\,{\rm nm}$ and $L_{\rm G} = 30\,{\rm nm}$ at $V_{\rm DS} = 0\,{\rm mV}$. Parameters: $\langle m_{\rm qu}^{\rm 1D}\rangle = 0.07\,{\rm m}_0$, WF = 4.77 eV, and $\alpha_{\rm np} = 1.2\,{\rm eV}^{-1}$.

Fig. 6 presents the results for $L_{\rm G} = 15\,{\rm nm}$. As in the 2DEG case, the slope of the QTx-curve cannot be reproduced without a quantum correction in S-Device. The anisotropic DG model in transport direction was applied

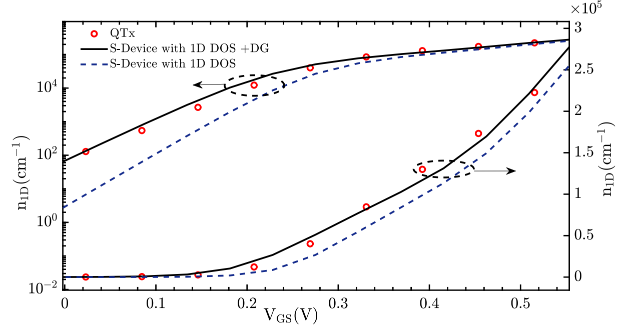

Figure 6: 1D electron density at the center of the channel vs. gate voltage in the GAA NW FET with $t_{\rm body} = 7\,{\rm nm}$ and $L_{\rm G} = 15\,{\rm nm}$ at $V_{\rm DS} = 0\,{\rm mV}$. Parameters: $\langle m_{\rm qu}^{\rm 1D}\rangle = 0.09\,{\rm m}_0$, $\gamma = 0.77$, $(\alpha_{\rm l}, \alpha_{\rm v}) = (1, 0)$, WF = 4.8 eV, and $\alpha_{\rm np} = 1.2\,{\rm eV}^{-1}$.

with a fitted $\alpha_{\rm l}$ value.

2.3. Ballistic Mobility Model

In a first instance, to mimic the ballistic QTx case, a constant and artificially high diffusive mobility ($\mu_{\rm d}$) of $2.3\times 10^4\ {\rm cm}^2/{\rm Vs}$ was used in the simulations of the DG UTB FETs. In the analysis of the GAA NW FETs we applied a ballistic mobility model $\mu_{\rm b}$ [7] which substitutes for the missing inertia term in the current equation [11]. It reduces the current in ultra-short channel FETs thus improving the agreement with the QTx characteristics. In 1D it has the form

$$\mu_{\rm b}(x) = \frac{v_{\rm b}(x)}{\psi_{\rm n}'(x)}\,, \tag{8}$$

where the gradient of the QFP $\psi_{\rm n}'(x)$ is the driving force of the carriers in the channel and $v_{\rm b}(x)$ their mean velocity given by

$$\begin{aligned} v_{\rm b}(x) &= v_{\rm th}\sqrt{\tanh^2\left(\frac{qV_{\rm DS}}{2k_{\rm B}T}\right) + \frac{2q\psi_{\rm n}(x)}{k_{\rm B}T}} \\ &\approx v_{\rm th}\sqrt{1 + \frac{2q\psi_{\rm n}(x)}{k_{\rm B}T}}\,. \end{aligned} \tag{9}$$

Here, $\psi_{\rm n}(x) = \phi(x) - \frac{k_{\rm B}T}{q}\ln(n)$ is the QFP, $v_{\rm th} = \sqrt{k_{\rm B}T/m_{\rm c}}$ the 1D mean thermal velocity, and q the elementary charge. The second line in Eq. (9) turns out as soon as the source-drain voltage exceeds a few $k_{\rm B}T/q$ which makes $\mu_{\rm b}$ parameter-free. In S-Device this form (with 1 replaced by a fitting parameter) is available as Kinetic Velocity Model (KVM) [9]. Details of its derivation are given in Ref. [6].

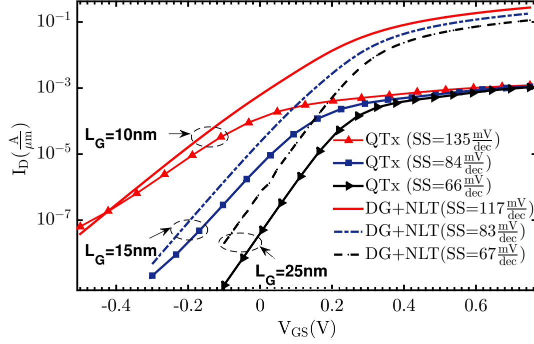

Figure 7: $I_D V_{GS}$-characteristics obtained from the combination of DG + NLT for a DG UTB FET with t_{body} = 7 nm and different gate lengths. Parameters: V_{DS} = 0.05 V, m_c = 0.0516 m$_0$, μ_d = 2.3×10^4 cm^2/Vs, γ = 0.7, (α_l, α_v) = (0,1), and WF = 4.8 eV.

3. Results

3.1. 3DEG DOS

Fig. 7 shows the fitted $I_D V_{GS}$-characteristics of the DG UTB FETs for three gate lengths computed with the combination of anisotropic DG model and NLT. Note that the 3DEG DOS model and Boltzmann statistics were used here, and that the mobility was set to a constant and large value to mimic the ballistic case.

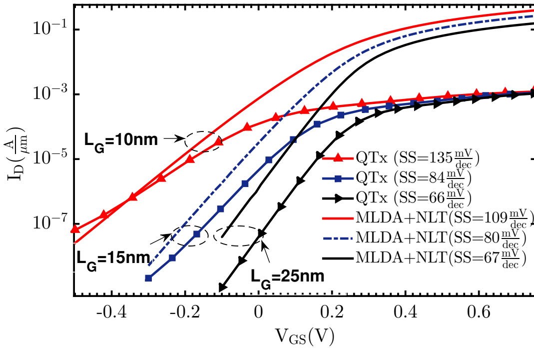

Figure 8: $I_D V_{GS}$-characteristics obtained from the combination of MLDA + NLT for a DG UTB FET with t_{body} = 7 nm and different gate lengths. Parameters: V_{DS} = 0.05 V, m_c = 0.0516 m$_0$, μ_d = 2.3×10^4 cm^2/Vs, and WF = 4.8 eV.

Neglecting Fermi statistics in the current equation, i.e. the term given in Eq. (7), as well as omitting the ballistic mobility correction Eq. (8) lead to a tremendous overestimation of the current density after the onset of inversion. This proves that both effects are essential to reproduce the on-current of the studied devices.

The *SS* of the transistor with the shortest L_G (where the effect of STDT is strongest) is best reproduced by the anisotropic DG model. Fig. 8 presents the $I_D V_{GS}$-characteristics for the DG UTB FETs using the combination MLDA + NLT. The slopes are similar to the previous case.

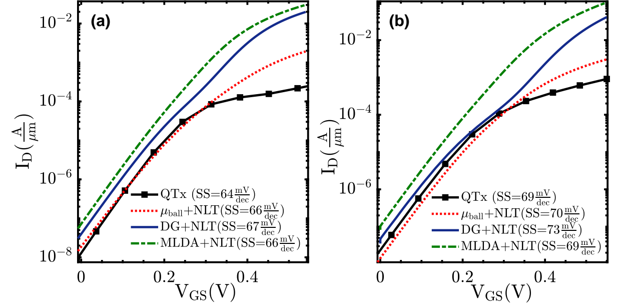

Figure 9: $I_D V_{GS}$-characteristics obtained from the combination of DG + NLT, MLDA + NLT and μ_b for a GAA NW FET with t_{body} =7 nm at (a) V_{DS} = 0.05 V and (b) V_{DS} = 0.63 V. Parameters: m_c = 0.0642 m$_0$, γ = 1.0, (α_l, α_v) = (0,1), and WF = 4.93 eV.

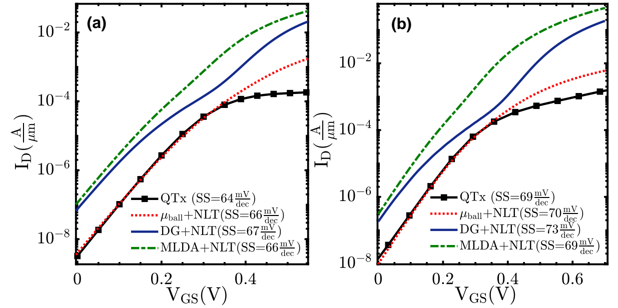

Figure 10: $I_D V_{GS}$-characteristics obtained from the combination of DG + NLT, MLDA + NLT and μ_b for a GAA NW FET with t_{body} = 5.5 nm at (a) V_{DS} = 0.05 V and (b) V_{DS} = 0.63 V. Parameters: V_{DS} = 0.05 V, m_c = 0.0674 m$_0$, γ = 1.0, (α_l, α_v) = (0,1), and WF = 4.98 eV.

Figs. 9 and 10 present the transfer curves of the GAA NW FETs from node A and B, respectively, in the linear regime (V_{DS} = 50 mV) and in the saturation regime (V_{DS} = 0.63 V). Again, the combinations DG + NLT and MLDA + NLT with a constant high mobility were used, but now also NLT in combination with the ballistic mobility Eq. (8). The following remarks have to be made: (i) Using the ballistic mobility together with the DG model never converges. Therefore, the electrostatics was corrected by a simple shift of the work function in this case. (ii) The apparent misfits in the threshold voltages between the DG and the QTx curves in Fig. 9 are not caused by the electrostatics, but due to the uncorrected constant mobility. (iii) The corresponding misfits in Fig. 10 are also due to a real difference between the

threshold voltages of DG and QTx curves, since the adjusted γ-value for $t_{body} = 5.5$ nm ($\gamma = 2$) prevented convergence, and $\gamma = 1$ was used instead.

The DG curves in Figs. 9 - 10 exhibit a pronounced bump around the onset of inversion. The strength of this effect increases with decreasing cross section of the GAA NW and increasing source-drain bias. It is attributed to the breakdown of the DG method when the channel quantization fades out and only geometrical confinement remains. The DG model had been developed for the former case, but is unable to cover the latter correctly. One can even observe the artifact that in the case of extremely thin bodies a huge quantum potential is computed in the flat-band regions of the semiconductor (also when $\alpha_l = 0$). An empirical workaround to mitigate this effect is to remove the gate oxide in small parts near the source/drain contacts [16] which eliminates the "density gradient" between insulator and semiconductor there. However, this was not done in the present study.

Applying the NLT model for STDT and the ballistic mobility model Eq. (8) in combination with a proper WF removes the bumps and yields an overall better agreement with the QTx transfer curves, except for the inversion range, and here especially in the linear regime. From the extracted *SS* values in Figs. 9 - 10 one observes that despite the superior electrostatic control in the GAA NWs, a significant leakage current caused by STDT persists. The best way to illustrate its effect is by showing the spectral current distribution in comparison to the shape of the lowest CB edge. This is done in Fig. 11 for the off-state and the on-state, respectively, comparing the gate lengths 15 nm and 10.5 nm. The on-current is basically thermionic current in both cases, i.e. STDT has no effect here. The off-current is dominated by STDT - almost completely in the case of L_G = 10.5 nm. Therefore, a gate length of 10 nm can be considered as the end of scaling for III-V-channel FETs. Further scaling will also not significantly improve the on-current.

3.2. 2DEG and 1DEG DOS

In the previous subsection the default S-Device DOS model of a 3DEG and Boltzmann statistics were used. In this subsection, Fermi statistics and the DOS models for a 2DEG/1DEG are applied. As discussed above, Fermi statistics is needed since the quasi-Fermi level is way higher than the lowest sub-band energy in the studied transistors. The Fermi correction term in the current equation (7) reduces the current in the inversion regime significantly. This effect increases with decreasing dimensionality, i.e. it is stronger for a

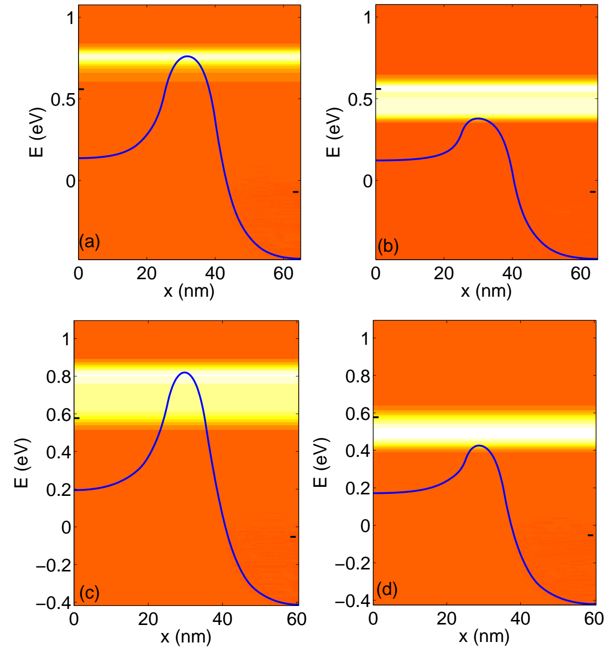

Figure 11: Distribution of spectral currents and lowest conduction band edge for GAA NW FETs from node (A) and (B) at V_{DS} = 0.63 V. (a) Off-state, L_G = 15 nm at V_{GS} = 0.026 V. (b) On-state, L_G = 15 nm at V_{GS} = 0.48 V. (c) Off-state, L_G = 10.4 nm at V_{GS} = 0.03 V. (d) On-state, L_G = 10.4 nm at V_{GS} = 0.48 V.

1DEG than for a 2DEG [17]. Fig. 12 shows the fitted $I_D V_{GS}$-characteristics of DG UTB FETs for three gate lengths computed with the combination of anisotropic DG model and a 2DEG DOS with the fitting parameters obtained from Figs. 2 and 3. As in the previous subsection, the mobility is constant and large here, without any ballistic correction. Anisotropic DG with fitted α_l is able to reproduce the slopes of the QTx-characteristics very well. The same can be achieved with the NLT model. The ballistic mobility correction would scale all currents down. However, the combination ballistic mobility + anisotropic DG does not converge.

Fig. 14 presents the transfer curves in the linear regime for a GAA NW from node A with a sufficient gate length (L_G = 30 nm) to avoid STDT. The combination 1DEG DOS + μ_b accounts both for the Fermi and mobility correction and reproduces the QTx curve reasonably well. The remaining difference in the on-current at V_{DS} = 0.05 V has its origin in the KVM-form Eq. (9) [7] and requires an empirical extension of the ballistic mobility model [6].

When working in the single-valley mode of S-Device, the STDT sub-threshold current obtained from QTx can always be reproduced with S-Device by a proper fit of

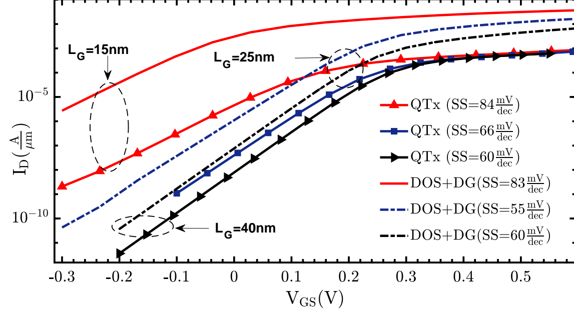

Figure 12: $I_D V_{GS}$-characteristics obtained from the combination of 2DEG DOS + the anisotropic DG for a DG UTB FET with t_{body} = 7 nm and different gate lengths. Parameters: V_{DS} = 0.05 V, $\mu_d = 2.3 \times 10^4\,\mathrm{cm^2/Vs}$, $\gamma = 0.77$, and $(\alpha_1, \alpha_v) = (1{,}0)$. The mass parameter $\langle m_{qu}^{2D} \rangle$ reduces from 0.038 m_0 for L_G = 40 nm to 0.027 m_0 for L_G = 15 nm.

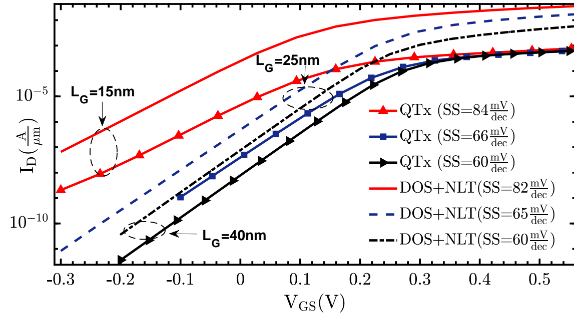

Figure 13: $I_D V_{GS}$-characteristics obtained from the combination of 2DEG DOS + NLT for a DG UTB FET with t_{body} = 7 nm and different gate lengths. All other parameters are the same as in Fig. 12.

the tunneling mass m_c. In the 'Multivalley' mode the same statement ('Multivalley') can also be used for the NLT model. Then the STDT current becomes the sum of the tunneling currents of all sub-bands included in the simulation, with the specified effective masses $m_{qu,i}^{1D,2D}$ as tunneling masses. This has been done in Fig. 15 and Fig. 16, which show the transfer curves in the linear and saturation regime of GAA NWs from node A and B, respectively. Again, the combinations 1DEG DOS and 1DEG DOS + NLT with a constant high mobility were used, but now also 1DEG DOS in combination with the ballistic mobility Eq. (8). The tunneling mass m_c used for each sub-band is exactly the same $\langle m_{qu}^{1D} \rangle$ as obtained before by fitting the electrostatics (compare Fig. 6). This value is too large to have a noticeable effect on the SS as can be seen by the comparison of the dashed green and the solid black curves. On the other hand, since the value is still smaller than the actual quantization masses $m_{qu,i}^{1D}$ close to the Fermi level, we attribute the discrepancy to the analytical form of the

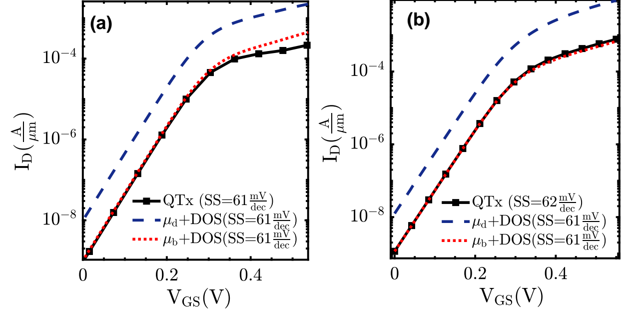

Figure 14: $I_D V_{GS}$-characteristics obtained from the combination of DG + 1DEG DOS, and μ_b + 1D DOS for a GAA NW FET with t_{body} =7 nm and L_G =30 nm. Parameters: $\langle m_{qu}^{1D} \rangle$ = 0.07 m_0, WF = 4.77 eV, and α_{np} = 1.2 eV^{-1}.

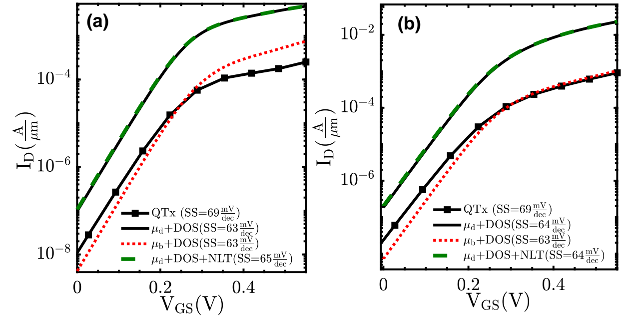

Figure 15: $I_D V_{GS}$-characteristics obtained from the combinations 1DEG DOS, 1DEG DOS + μ_b, and 1DEG DOS + NLT + μ_d for a GAA NW FET with t_{body} =7 nm (node A) at (a) V_{DS} = 0.05 V and (b) V_{DS} = 0.63 V. Parameters: α_{np} = 1.2 eV^{-1}, $m_c = \langle m_{qu}^{1D} \rangle = 0.09\, m_0$, and WF = 4.8 eV.

NLT model in S-Device which was derived for a 3DEG.

Tables 2 and 3 summarize the results and show how the use of a large diffusive mobility without ballistic correction overestimates the on-current drastically and how the combination 1DEG DOS + μ_b from Eq. (8) improves the situation. Also in the 1DEG case, the on-current is much better reproduced in the saturation than in the linear regime. The reasons for this are discussed elsewhere [7].

4. Conclusion

With a 3DEG DOS, the NLT model used in combination with the anisotropic DG model, applied to the vertical direction, can fairly reproduce the reference *SS* of the DG UTB FETs in the case of strong STDT. Also with a 2DEG DOS, the anisotropic DG model (applied to the transport direction) and the NLT model yield similar slopes as obtained from QTx. In GAA NW FETs

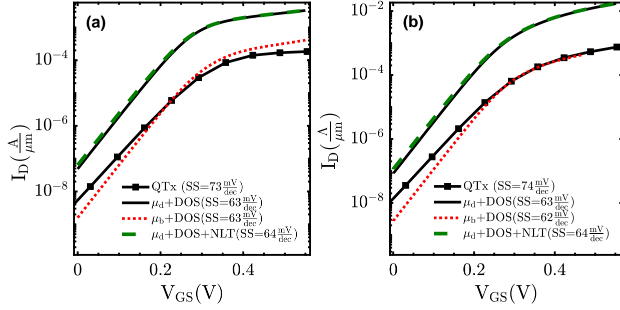

Figure 16: $I_D V_{GS}$-characteristics obtained from the combinations 1DEG DOS, 1DEG DOS + μ_b, and 1DEG DOS + NLT + μ_d for a GAA NW FET with t_{body} =5.5 nm (node B) at (a) V_{DS} = 0.05 V and (b) V_{DS} = 0.63 V. Parameters: α_{np} = 1.1 eV^{-1}, $m_c = \langle m_{qu}^{1D} \rangle = 0.08\, m_0$, and WF = 4.77 eV.

Table 2: Extracted on-current I_{ON} at V_{GS} = 0.5 V and V_{DS} = 0.05 V. All current densities are in units of A/μm.

Node	I_{ON}(QTx)	$I_{ON}(\mu_b)$	$I_{ON}(\mu_b)$ + *DOS*	I_{ON}(DG+NLT)
A	1.7×10^{-4}	1.56×10^{-3}	5.2×10^{-4}	1.7×10^{-2}
B	1.7×10^{-4}	1.8×10^{-3}	3.3×10^{-4}	1.8×10^{-2}

Table 3: Extracted on-current I_{ON} at V_{GS} = 0.5 V and V_{DS} = 0.63 V. All current densities are in units of A/μm.

Node	I_{ON}(QTx)	$I_{ON}(\mu_b)$	$I_{ON}(\mu_b)$ + *DOS*	I_{ON}(DG+NLT)
A	7.7×10^{-4}	2.6×10^{-3}	7.7×10^{-4}	2.7×10^{-2}
B	5.3×10^{-4}	1.5×10^{-3}	5.3×10^{-3}	1.3×10^{-2}

the excellent gate electrostatic control reduces *SS* significantly compared to the DG UTB FETs with the same L_G [12]. Application of a ballistic mobility model in combination with the 1DEG DOS yields an overall good agreement with the QTx transfer curves after the onset of inversion and decreases I_{ON} by two orders of magnitude in comparison to the simulation with a large diffusive mobility. However, the SS degradation due to STDT can not be reproduced with the same quantization mass that fits the electrostatics. To better understand the reasons it is necessary to revisit the NLT model for a 1DEG.

Acknowledgment

The research leading to these results was supported by the European Commissions Seventh Framework Programme (FP7/2007-2013) under Grant Agreement No. 619326 (III-V-MOS Project). The authors would like to thank O. Penzin (Synopsys USA) for the implementation of low-dimensional DOS models in S-Device and for valuable discussions and technical advice.

References

[1] J. A. del Alamo, Nanometer-scale electronics with III-V compound semiconductors, *Nature*, vol. 479, pp. 317-322, 2011.

[2] A. Wettstein, A. Schenk, and W. Fichtner, "Quantum device-simulation with the density-gradient model on unstructured grids", *IEEE Trans. on Electron Devices*, vol. 48, no. 2, pp. 279-284, 2001.

[3] F. O. Heinz, A. Schenk, "Self-consistent Modeling of Longitudinal Quantum Effects in Nanoscale Double-gate Metal Oxide Semiconductor Field Effect Transistors", *Jour. Appl. Phys.*, vol. 100, 084314, 2006.

[4] P. Aguirre, H. Carrillo-Nunez, A. Ziegler, M. Luisier, and A. Schenk, "Drift-diffusion quantum corrections for $In_{0.53}Ga_{0.47}As$ double gate ultra-thin-body FETs", *Proc. of Int. Conf. on Simulation of Semiconductor Processes and Devices (SISPAD)*, pp. 53-56, 2016.

[5] Sentaurus-Device Monte Carlo (S-Band) User Guide, V-2016.03, Synopsys Inc., Mountain View, California, 2016.

[6] O. Penzin, L. Smith, A. Erlebach, M. Choi, and K.-H. Lee, "Kinetic Velocity Model to Account for Ballistic Effects in the Drift-Diffusion Transport Approach", *IEEE Trans. on Electron Devices* vol. 64 (11), 4599 - 4606, 2017.

[7] P. Aguirre and A. Schenk, "Ballistic Mobility Model for QDD Simulation of Ultra-short Transistors", *Proc. of Electron Devices Technology ad Manufacturing Conference (EDTM)*, Kobe, pp. 77 - 79, 2018.

[8] A. Ziegler; M. Frey; L. Smith; M. Luisier, "A Nonparabolic Bandstructure Model for Computationally Efficient Quantum Transport Simulations", IEEE Trans. Electron Devices, vol. 63 (5), pp. 2050 - 2056, 2016.

[9] Sentaurus S-Device User Guide, version N-2017.09, Synopsys Inc., Mountain View, California, 2017.

[10] M. Luisier, A. Schenk, and W. Fichtner, "Atomistic simulation of nanowires in the $sp^3d^5s^*$ tight-binding formalism: From boundary conditions to strain calculations", Phys. Rev. B 74, 205323, 2006.

[11] W. R. Frensley, "Barrier-limited Transport in High Electron Mobility Transistors" , IEEE Trans. on Electron Devices, vol. 30 (12), pp. 1619-1623, 1983.

[12] M. Rau, E. Caruso, D. Lizzit, P. Palestri, D. Esseni, A. Schenk, L. Selmi, and M. Luisier, "Performance projection of III-V ultra-thin-body, FinFET, and nanowire MOSFETs for two next-generation technology nodes", *IEDM Tech. Digest*, San Francisco, pp. 758-761, 2016.

[13] A. Schenk and A. Wettstein, "Simulation of DGSOI MOSFETs with a Schrödinger-Poisson based mobility model", *Proc. of Int. Conf. on Simulation of Semiconductor Processes and Devices (SISPAD)*, pp. 21-24, 2002.

[14] M. Luisier, A. Schenk, and W. Fichtner, "Quantum transport in two- and three-dimensional nanoscale transistors: Coupled mode effects in the nonequilibrium Green's function formalism", *Jour. Appl. Phys.*, vol. 100, 043713, 2006.

[15] O. Penzin, G. Paasch and L. Smith, "Nonparabolic Multivalley Quantum Correction Model for InGaAs Double-Gate Structures," *IEEE Trans. on Electron Devices*, vol. 60, no. 7, 2246 - 2250, 2013.

[16] A. Erlebach, Synopsys Switzerland LLC, private communication.

[17] O. Penzin, Synopsys USA, private communication.

[18] G. Zerveas, E. Caruso, G. Baccarani, L. Czornomaz, N. Daix, D. Esseni, E. Gnani, A. Gnudi, R. Grassi, M. Luisier, T. Markussen, P. Osgnach, P. Palestri, A. Schenk, L. Selmi, M. Sousa, K. Stokbro, and M. Visciarelli, ”Comparison of modeling approaches for band-structure calculation in III-V semiconductor quantum wells”, Solid-State Electronics 116, pp. 92 - 102, 2016, doi:10.1016/j.sse.2015.09.005.

[19] Sentaurus-Device User Guide, version N-2019.03, chapter 12, Synopsys Inc., Mountain View, California, 2018.